Int. J. Electrochem. Sci., 13 **(2018)** 6248 – 6258, doi: 10.20964/2018.07.46

International Journal of
ELECTROCHEMICAL
SCIENCE
www.electrochemsci.org

Electrochemical Analysis of Carbon Steel Corrosion Induced by Chloride and Sulfate Ions in Simulated Concrete Pore Solution

Guojian Liu, Yunsheng Zhang[*], *Meng Wu, Yu Zhang, Bo Pang*

School of Materials Science and Engineering, Southeast University, Nanjing 211189, China
[*]E-mail: liuguojiande@gmail.com zhangyunsheng2011@163.com

Received: 2 March 2018 / *Accepted:* 8 May 2018 / *Published:* 5 June 2018

In this study, the corrosion process of steel reinforcement induced by chloride and/or sulfate ions was investigated by electrochemical measurements and theoretical analysis. Electrochemical impedance spectroscopy as a powerful and revealing tool was adopted to monitor and interpret the corrosion process with experiment time lapse. Detailed information on the parameters of passive film in different corrosion phases was obtained via the proposed electrochemical equivalent circuit simulation. The results indicated that increasing sulfate ions could initiate corrosion. Furthermore, sulfate showed higher corrosion risk than chloride as per amount of substance of aggressive anions in the simulated concrete pore solution. The presence of both chloride and sulfate ions led to higher corrosion rate than that of the exposed to chloride or sulfate ions alone. The Nyquist curve, Bode modulus, and phase angel format of the EIS data revealed more detailed information regarding each stage of corrosion. The Chi-square (χ^2) value method was adopted for the verification of the fitted results by the proposed equivalent circuit.

Keywords: Carbon steel; Corrosion; Electrochemical analysis; Chloride; Sulfate

1. INTRODUCTION

Reinforced concrete structures have found increasing applications and service in demanding environment including ports, piers, and offshore engineering infrastructures. As large-scale infrastructure construction has been taking place in China, the reinforced concrete structures in northwest districts and South China sea areas are susceptible to severe deterioration induced by steel corrosion, as corrosion is an omnipresent issue in most infrastructure applications. The corrosion alone costs $2.5 trillion each year globally, equivalent to roughly 3.4% of the global GDP [1]. In a recent study, the annual cost of corrosion in China was estimated to be ~2127.8 billion RMB (~310 billion USD) [2]. Thus, a better understanding of corrosion is essential for mitigating or avoiding catastrophic metal failure, substantial economic loss, and even life in the most serious cases.

Reinforcing steels embedded in cementitious materials are basically inert to corrosion, because of the formation of a thin protective film in high alkaline environment surroundings. However, active corrosion of steels is initiated when chloride is accumulated to a certain extent in the vicinity of steels [3–5]. Numerous reinforced concrete structures in many places such as northwest districts of China [6], salinized soil area in the Arabian Gulf region [7, 8], marine engineering [9, 10], and underground water and industrial scenarios are exposed to demanding service conditions with chloride coupled by concentrated sulfate ions. Couples of studies have been conducted in regard to durability issues caused by chloride or sulfate ions [11–15].

While the effect of chlorides on reinforcing steel corrosion as well as the internal or external sulfate attack to the matrix of cementitious materials is well documented in the literature, the corrosion behavior of steels subjected to sulfate ions or concurrent existence of chloride and sulfate has been scarcely reported. Dehwah *et al*. [16, 17] investigated reinforced concrete samples exposed to chloride plus sulfate solutions and found that the presence of sulfate ions negligibly affected the corrosion potential, but increased the corrosion current density. Earlier research [18] reported the increase in corrosion current to rate-limiting factors of sulfate ions in different corrosion periods. Similar studies [19, 20] also showed that sulfate significantly increased the corrosion rates, but exerted a marginal effect on the corrosion initiation time. In early researches [21, 22], Al-Teyyib *et al*. studied the effect of sulfate on the corrosion behavior of steel in saturated $Ca(OH)_2$ and concrete. Sulfate ions were also found to be corrosive to steels but to a lesser extent than chloride. Notably, sulfate ions were premixed into fresh concrete and could change the chemical properties of hardened concrete pore solution; therefore, affecting the passivation and depassivation of steels. However, in recent studies, Pradhan *et al*. admixed varying contents of chloride and composite chloride–sulfate ions in concrete and prepared an electrolytic concrete powder solution by the leaching method [23, 24]. Their research indicated that sodium sulfate inhibited steel corrosion to some extent, whereas magnesium sulfate facilitated the reinforcement corrosion induced by chloride. In addition, Espinosa-Medina *et al*. [25] investigated the stress corrosion cracking of weldments in the presence of chloride and sulfate and found that the addition of chloride increased the corrosion activity, but the additions of sulfate ions led to the formation of a passive layer on the metallic surface. In addition, Niu *et al*. [26, 27] studied the corrosion behavior of ^{13}Cr steel in simulated boiler water containing chloride and sulfate ions. The authors reported that pitting initiation impressed when sulfate content reached 50 ppm and conversely became promoted at a high concentration of 100 ppm. However, this was found to be in contrast to the study of other researchers [28] who reported that such a high SO_4^{2-} content as 0.5 or 1 mol/L could also inhibit corrosion aroused by Cl^- as well. Furthermore, no consensus has been obtained either on the experimental design, configurations, or the role of sulfate ions on the steel reinforcement corrosion among the available literature. This directly leads to the wide scatter in research conclusions in the literature or even entirely different opinions.

Electrochemical impedance spectroscopy (EIS) has been a powerful analysis tool to monitor and interpret the corrosion process of metal in different cases. Further, a saturated solution of $Ca(OH)_2$ could well represent concrete pore solution environment, as many researchers [29–32] conducted their study in saturated $Ca(OH)_2$ as a simulated concrete pore solution. This preliminary study aimed to

investigate the role of sulfate ions on the corrosion behavior in simulated concrete pore solution. The corrosion process was analyzed by electrochemical methods including open circuit potential, corrosion current density, and especially EIS.

2. EXPERIMENTAL

2.1 Preparation of steel samples and exposure solution

Tested carbon steel specimens with a size of Φ16×10 mm were cut from a steel rod. The chemical composition (wt) of the steel specimens is as follows: 0.20% C, 0.55% Si, 1.42% Mn, 0.028% S, 0.026% P, and balance Fe. A copper wire welded to one cross-section surface for electrochemical link. This welded cross-section surface and the cylindrical surface were carefully sealed by epoxy resin. The remaining cross-section surface was polished gradually using silicon carbide paper to grit 1000 as the tested surface and then degreased by acetone and washed with distilled water.

The simulated concrete solution of saturated $Ca(OH)_2$ was prepared using deionized water with some insoluble solute. NaCl and Na_2SO_4 were added incrementally as aggressive ions. All the reagents used in this study were of analytical reagent grade.

2.2 Electrochemical techniques

All the samples were divided into three groups, namely, Group A, B and C. All the samples were pre-passivated in saturated calcium hydroxide solution for 10 d to reach a stable passivation state prior to test. When a stable condition was achieved, electrochemical tests were performed using PARSTAT4000 immediately before each addition of aggressive ions each day. Grouping of samples and incremental additions of aggressive ions are listed in Table 1. A classic three-electrode system was adopted with the tested steel samples, saturated calomel electrode (SCE), and platinum electrode as the working electrode, reference electrode, and counter electrode, respectively. The corrosion current density (Icorr) was calculated by the linear polarization method in regard to the Stern–Geary method [33] as shown by Equation 1:

$$I_{\text{corr}} = \frac{B}{R_{\text{p}}} = \frac{1}{R_{\text{p}}} \frac{\beta_{\text{a}}\beta_{\text{c}}}{2.303(\beta_{\text{a}}+\beta_{\text{c}})} \quad (1)$$

where I_{corr} is the corrosion rate of current density, Rp the polarization resistance, B the Stern-Geary constant that is a function of β_a and β_c, where β_a and β_c are anodic and cathodic Tafel slope, respectively. The value of B is reported to range from 26 to 52 mV [34] and 26 mV was adopted herein. EIS test was conducted with a perturbation amplitude of 10 mV, from 10^5 Hz to 10^{-2} Hz. Corrosion potential (Ecorr) was determined after steady open circuit potential was obtained. In linear polarization resistance (LPR) tests, tested samples were polarized to ±10 mV vs Ecorr and the scanning rate is 0.166 mV/s.

Table 1. Grouping of steel samples and stepwise additions of aggressive ions

Group	Aggressive ions	Addition
Group A	NaCl	0.01 mol/L per day
Group B	Na_2SO_4	0.01 mol/L per day
Group C	NaCl+ Na_2SO_4	0.60(fixed)+0.01 mol/L per day

2.3 Proposed equivalent circuit

In a previous discussion [31], principles to select suitable equivalent circuit for simulation of experimental EIS results. Bearing the topology approaching principle in mind, quantitative calculation using Chi-square (χ^2) value method was supposed to be performed. Above all, the physical meaning and evolution trend of the simulated parameters according to the chosen equivalent circuit shall stand. Based on these principles, the equivalent circuit of $R_s(Q_f(R_f(Q_{dl}R_{ct})))$ was proposed in present study. To obtain accurate results, the capacitance elements are all replaced by constant phase elements (CPE), namely Q_f and Q_{dl} in Fig. 1. Rs represents the solution resistance and Q_f the capacitive behavior of passive film. R_f deals with the ionic resistance through the passive film. Q_{dl} is the capacitive behavior of double layer of localized corrosion area while Rct stands for the charge transfer resistance. The impedance Z_{CPE} of Q is defined as follows: $z_{CPE}=Y_0^{-1}(j\omega)^{-n}$. Y_0 is the capacitance value of CPE, ω is the angular frequency, j is the imaginary number and n is the CPE exponent.

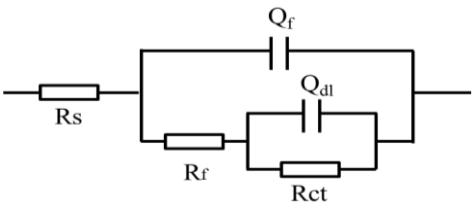

Figure 1. Schematic diagram of proposed equivalent circuit.

3. RESULTS AND DISCUSSION

3.1 Ecorr and Icorr

The evolution of Ecorr and Icorr of all the samples is shown in Figure 2. As depicted in the Figure 2(a), the initial Ecorr after 10d of pre-passivation ranges between −200 mV to −240 mV with reference to SCE. Then, Ecorr shifts towards a more negative direction with increasing contents of chloride and/or sulfate ions. Particularly, samples subjected to chloride show a dramatic drop when chloride content rises around 0.05 mol/L, whereas sulfate ions leads to a more severe decrease in Ecorr. In Group C, with the first addition of 0.60 mol/L chloride and 0.01 mol/L sulfate, the Ecorr decreases to −450 mV, indicating a higher risk of corrosion.

While Ecorr reflects corrosion thermodynamics, Icorr shows the reaction kinetics of passive film. Figure 2(b) shows that Icorr increases with increasing stepwise additions of aggressive ions. At critical concentrations, the localized thinning of passive film is sufficient to give rise to dielectric breakdown of passive film and occurrence of pitting corrosion. The corrosion reaction occurred at a higher rate in the absence of the protective film. In addition, sulfate ions lead to higher corrosion current density than chloride especially when sulfate content exceeds 0.03 mol/L. It is inferred that sulfate ions modified the original iron oxide film to a less inhibitive ferric sulfate compounds film [21, 35], yet other researchers [36] ascribed this higher corrosion rate to high conductivity because sulfate ions carried larger number of charges at the same molar concentration compared to chloride. Samples of Group C denote the highest corrosion rate, partially because the first addition of chloride is too high. However, it should be noted that along with following increase of sulfate, the Ecorr and Icorr still shift towards more severe corrosion direction. Conductive electric charge in the presence of one mole of sodium sulfate is several times of that of one mole of sodium chloride, probably favoring the current flow within the corroded areas of the steel. However, it is believed that sulfate ions, similar to chloride ions, act as catalysts to convert iron atoms to ferrous ions, inducing active corrosion and dissolution of the original passive film, as confirmed by other researchers [37, 38]. Additionally, in scenario of Group C with both chloride and sulfate ions, the lowest Ecorr and highest corrosion current density was observed. However, the type of corrosion products did not change and remained with a reference to research conducted by Wu *et al* [39].

With regard to corrosivity between chloride and sulfate ions, some interesting phenomena could be observed. In Group B and C, with incremental additions of aggressive ions, Ecorr shift decreases and Icorr increases. When at the same content, sulfate lead to more negative Ecorr and higher Icorr than chloride ions. Similar evolution is also found by Haleem and Aal [40-42].

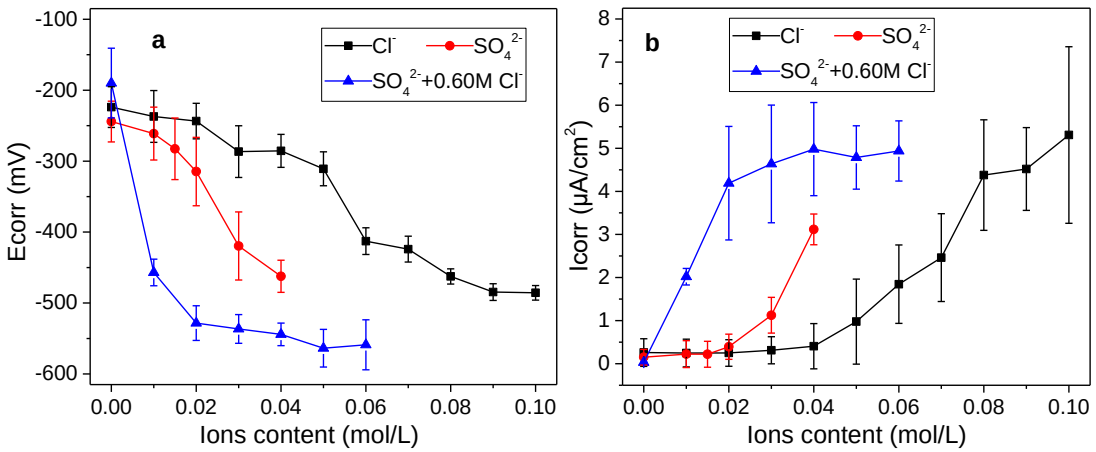

Figure 2. Ecorr and Icorr evolution of samples with increasing contents of ions: (a)Ecorr (b)Icorr.

3.2 Electrochemical impedance spectroscopy

EIS is commonly utilized as a powerful and versatile tool to investigate the mechanisms of electrochemical reactions, dielectric properties of electrodes, passivation process, and so forth [31, 43,

44]. The basic principle is to apply an alternating electrical signal of small magnitude to the test system at the steady state and record the electrical response of the system to external perturbation. Over a wide range of frequency, different types of circuit elements are supposed to show unique response. In this sense, detailed information regarding the tested system can be obtained. The typical EIS plots in the Nyquist format are shown in Figure 3. The symbols stand for the measured experimental data, and solid lines represent simulated results. A series of depressed "semicircles" are shown in Figure 3, arising due to the fact that the testing was only conducted within 10^5 Hz to 10^{-2} Hz. Gradual decreasing trend of the semicircle radius with increasing additions of chloride turns out a dramatic dropdown when the content exceeds 0.05 mol/L. This sharp reduction in the charge transfer resistance of passive film reveals an increased corrosion possibility. When it comes to sulfate ions in Group B, the threshold value is between 0.02 and 0.03 mol/L, much lower than that of chloride. In Figure 3(c), the topology of the Nyquist curve discloses a marked compaction after the initial addition of high content of chloride, simulating the demanding service environment of marine or offshore engineering. However, it is obvious that with the later incremental addition of sulfate ions, the capacitive arc as well as the radius of curvature maintained compacting trend, indicating an ever-increasing corrosion risk.

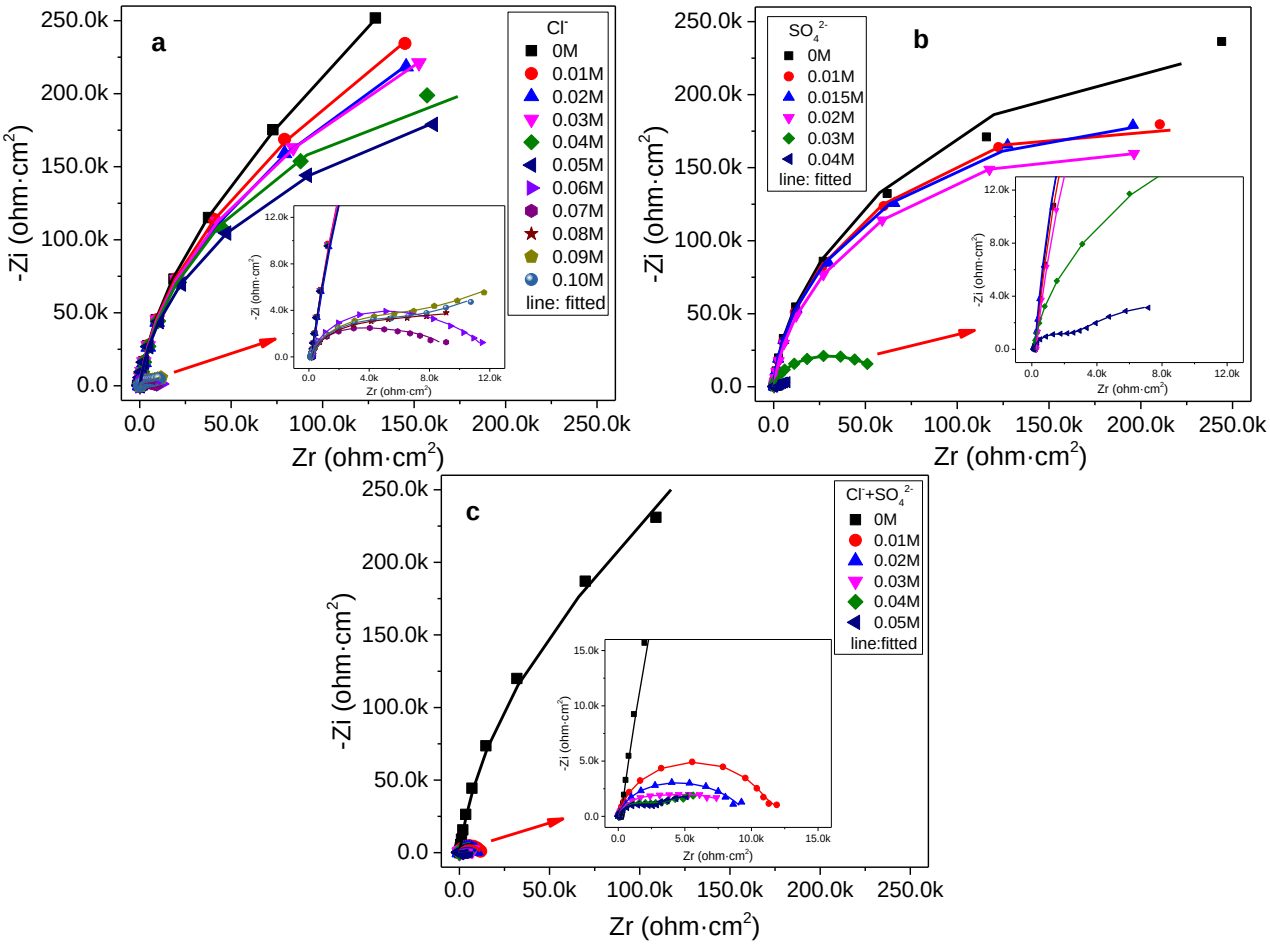

Figure 3. Typical Nyquist plots of steel samples with increasing contents of ions: (a) Group A, (b) Group B, (c) Group C.

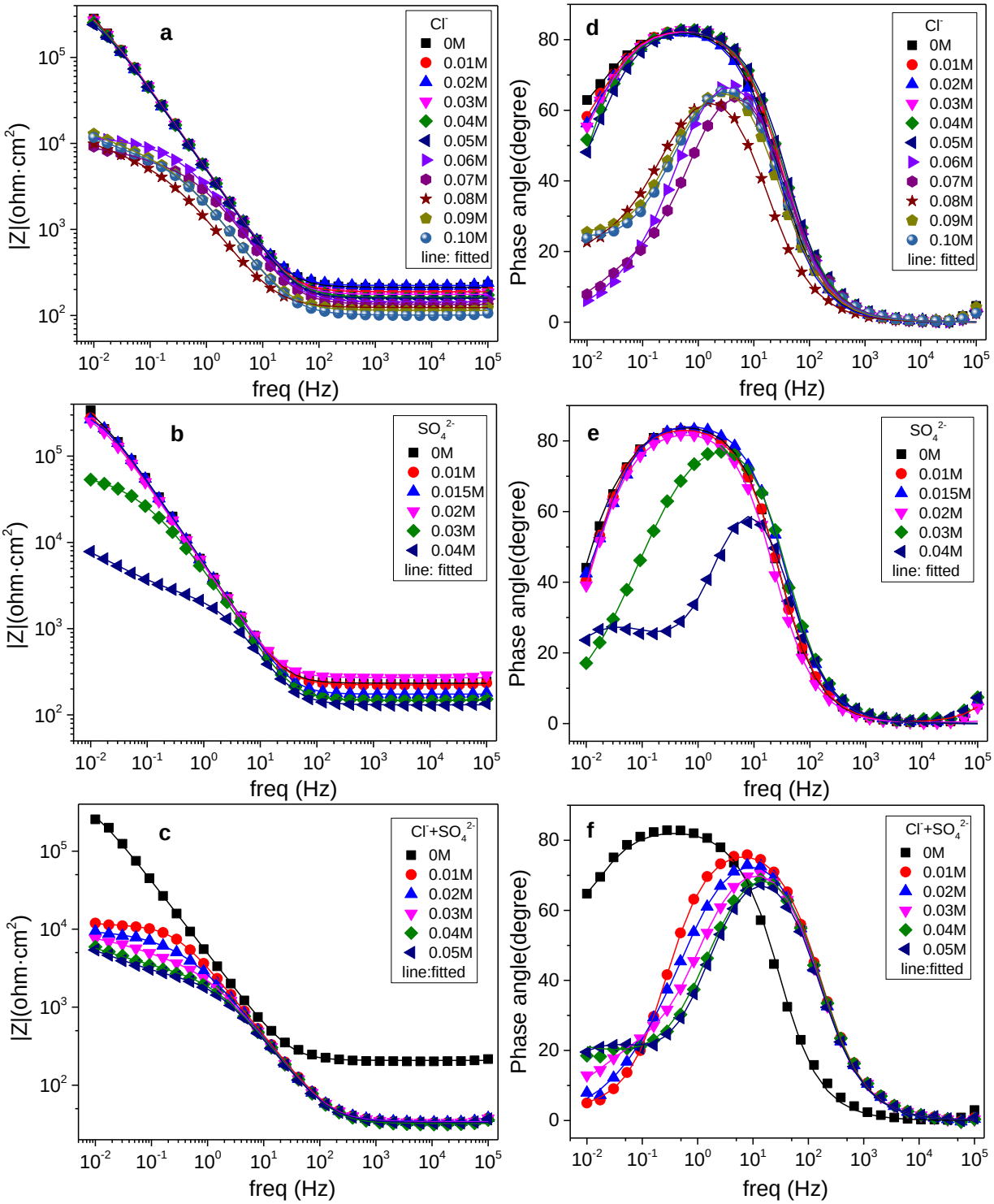

Figure 4. Bode modulus and phase angle spectrum of steel samples with increasing contents of ions: (a)Bode modulus of Group A, (b)Bode modulus of Group B, (c)Bode modulus of Group C, (d) phase angle spectrum of Group A, (e) phase angle spectrum of Group B, (f) phase angle spectrum of Group C.

The Bode modulus (Z vs. frequency) and phase angle spectrum (phase angle vs. frequency) of steel samples are demonstrated in Figure 4. The topology of all the plots shows a relatively high fitting degree between the experimental data and simulated results. In the Bode format, the curve reveals a

flat land in the high frequency domain. Modulus within this range represents the electrolyte resistance, and with increasing additions of aggressive ions, the electrolyte resistance maintains a reducing trend because of upscaling solution conductivity. Modulus within the lowest frequency domain is related to the charge transfer resistance as is the semicircle radius in Nyquist plots, serving as an estimation of the corrosion protection of the film. In Figure 4(a), the modulus value at 0.01 Hz manifests a sudden dropdown of over one magnitude of order when the chloride content reaches 0.05 mol/L. Figure 4(b) shows a decrease of one order of magnitude at 0.02 and 0.03 mol/L of sulfate ions. The electrolyte resistance and Rct significantly decreased when exposed to the salts.

Figures 4(d), (e) and (f) depict the phase angle vs. frequency of samples in Groups A, B, and C, respectively. Mostly, only one time constant can be observed in abovementioned figures except that two peaks occur at 0.04 mol/L in Figure 4(e) and 0.04 and 0.05 mol/L in Figure 4(f). This phenomenon could be attributed to Warburg element representing semi-infinite length diffusion process with much corrosion products being accumulated. However, the Warburg diffusion has not been considered in order to ensure the consistency in this study. The phase angle value within the middle frequency range is associated with the integrity and protective property of passive film. The phase angles in the middle range and sub-middle range gradually decrease with increasing ion concentrations. Then, dramatic changes occur when it comes to threshold values. It could be intuitively seen that the incremental additions of chloride or sulfate clearly changed the Bode modulus spectrum and phase angle spectrum.

3.3 Equivalent circuit modelling and verification

Further in order to verify the accuracy of simulated results, Chi-square ($\chi 2$) value method [31, 45-47] was adopted as shown in the following equation 2 and 3:

$$\chi^2=\sum_{i=1}^{N}\frac{\left[Z_{re,exp}(\omega_i)-Z_{re,fit}(\omega_i)\right]^2+\left[Z_{im,exp}(\omega_i)-Z_{im,fit}(\omega_i)\right]^2}{\left|Z(\omega_i)\right|^2} \quad (2)$$

$$|Z(\omega_i)|=\sqrt{Z_{re,exp}(\omega_i)^2+Z_{im,exp}(\omega_i)^2} \quad (3)$$

where $Z_{re,exp}(\omega_i)$ and $Z_{im,exp}(\omega_i)$ are measured data of real part and imaginary part, respectively. $Z_{re,fit}(\omega_i)$ and $Z_{im,fit}(\omega_i)$ are corresponding fitted values. $|Z(\omega_i)|$ is the modulus of impedance as a weighing factor. It can be seen that Chi-square value implies the variance between measured data and fitted results, and lower χ^2 indicates a better quality of the fitting.

Table 2. Fitting results at different chloride contents.

Cl^- (mol/L)	Rs ($ohm\cdot cm^2$)	Q_f		R_f ($ohm\cdot cm^2$)	Q_{dl}		Rct ($ohm\cdot cm^2$)	Chi-square
		Y_0 ($S\cdot cm^{-2}\cdot sec^n$)	n		Y_0 ($S\cdot cm^{-2}\cdot sec^n$)	n		
0.00	212.3	3.558E-5	0.9355	5.286E5	4.912E-5	0.9856	5.765E5	9.960E-4
0.01	188.1	3.539E-5	0.9391	4.521E5	6.138E-5	0.9671	3.664E5	8.445E-4
0.02	223	3.67E-5	0.9344	4.366E5	6.868E-5	0.9678	2.58E5	9.321E-4
0.03	175.7	3.569E-5	0.9376	4.170E5	9.422E-5	0.9566	2.482E5	8.554E-

0.04	163.1	1.973E-5	0.9872	4.012E5	1.733E-5	0.8469	4.746E5	8.958E-4
0.05	158.5	3.632E-5	0.9373	3.409E5	1.564E-4	0.8999	1.31E5	9.804E-4
0.06	143.9	5.434E-5	0.8971	8558	6.166E-4	0.7160	3326	7.099E-4
0.07	134.6	5.612E-5	0.8974	5121	5.167E-4	0.6639	4521	7.152E-4
0.08	123.3	1.512E-4	0.8636	5313	5.403E-4	0.5217	14390	3.185E-4
0.09	114.2	8.874E-5	0.8863	5069	3.203E-4	0.3751	32440	7.237E-4
0.10	100.8	8.748E-5	0.8878	4666	3.485E-4	0.3621	72660	4.110E-4

Table 3. Fitting results at different sulfate contents.

SO_4^{2-} (mol/L)	Rs ($ohm \cdot cm^2$)	Q_f		R_f ($ohm \cdot cm^2$)	Q_{dl}		Rct ($ohm \cdot cm^2$)	Chi-square
		Y_0 ($S \cdot cm^{-2} \cdot sec^n$)	n		Y_0 ($S \cdot cm^{-2} \cdot sec^n$)	n		
0.00	233.1	2.973E-5	0.9619	3.733E5	6.323E-5	1	1.083E5	1.545E-3
0.01	0.04935	5.85E-10	1	223	3.177E-5	0.9929	3.819E5	3.781E-4
0.015	174.1	3.055E-5	0.9618	3.504E5	2.688E-4	0.9850	1.821E5	10.61E-4
0.02	252.6	2.49E-6	0.6411	19.42	3.032E-5	0.9580	3.705E5	5.667E-4
0.03	148.6	3.419E-5	0.9588	1.723E4	3.776E-5	0.5938	5.22E4	13.25E-4
0.04	131	4.556E-5	0.9355	2158	6.082E-4	0.5269	1.259E4	15.83E-4

Table 4. Fitting results at different sulfate contents with 0.60mol/L of chloride.

SO_4^{2-} (mol/L)	Rs ($ohm \cdot cm^2$)	Q_f		R_f ($ohm \cdot cm^2$)	Q_{dl}		Rct ($ohm \cdot cm^2$)	Chi-square
		Y_0 ($S \cdot cm^{-2} \cdot sec^n$)	n		Y_0 ($S \cdot cm^{-2} \cdot sec^n$)	n		
0.00	207.5.	3.697E-5	0.9328	6.939E5	5.719E-5	1	3.543E5	1.807E-3
0.01	34.07	5.459E-5	0.9055	1.138E4	4.329E-4	0.9573	8760	1.127E-3
0.02	34.37	5.792E-5	0.9035	5208	2.583E-4	0.6174	4564	1.167E-3
0.03	33.81	6.087E-5	0.897	3419	4.558E-4	0.5867	6019	1.013E-3
0.04	32.30	5.654E-5	0.910	1800	5.869E-4	0.3162	6211	1.592E-3
0.05	33.27	6.480E-5	0.8918	2244	9.988E-4	0.5877	6050	1.011E-3

The corrosion parameters as well as the Chi-square values of Groups A, B, and C simulated by the proposed equivalent circuit are listed in Tables 2, 3, and 4, respectively. Table 2 shows a general decreasing trend for Q_{dl} and Rct. Lower n indicates the breakdown of passive film and pitting readily occurs. The change of magnitudes of order in the value of Rct means active corrosion; however, Table 3 Rct reveals a sharp reduction from 3.705E5 to 5.22E4 with sulfate ion content changing from 0.02 to 0.03 mol/L, leading to a sharp increase in Icorr. Notably, n and Rct showed a small fluctuation, possibly because of the negligence of Warburg diffusion, which will be reported in the near future. In general, the Chi-square values of Groups A and B are within an order of magnitudes of 10^{-4}, showing a good consistency with the curves in Figures 3 and 4, whereas those of samples in Group C were between 1.011E-3 and 1.807E-3. According to topology in Figures 3 and 4 and mostly good order of simulated parameters of each element, the proposed circuit of $R_s(Q_f(R_f(Q_{dl}R_{ct})))$ is appropriate for the fitting of EIS.

4. CONCLUSION

In conclusion, electrochemical monitoring and analysis of steel corrosion induced by chloride and sulfate ions in simulated concrete pore solution were investigated. The abovementioned results and discussion indicate that chloride ions induce corrosion of steel at an approximate content of 0.05 mol/L. Sulfate alone can also initiate the steel corrosion in simulated concrete solution; however, its threshold content is relatively lower than chloride, indicating a higher corrosion risk in certain cases. The chi-square (χ^2) value method was found as an effective verification measure to ensure valid simulation and interpretation of EIS data.

ACKNOWLEDGEMENT
The authors gratefully acknowledge financial support from 973 Program (2015CB655102) and Natural Science Foundation of China (51678143).

References

1. G. Koch, J. Varney, N. Thompson, O. Moghissi, M. Gould and J. Payer, International Measures of Prevention, Application, and Economics of Corrosion Technologies Study, NACE International, (2016) Houston, USA.
2. B. Hou, X. Li, X. Ma, C. Du, D. Zhang, M. Zheng, W. Xu, D, Lu and F. Ma, npj Mater. Degrad., 1 (2017) 4.
3. U. Angst, B. Elsener, C. K. Larsen and Ø. Vennesland, *Cem. Concr. Res*., 39(2009)1122.
4. R.B. Figueira, A. Sadovski, A.P. Melo and E.V. Pereira, *Constr. Build. Mater*., 141(2017)183.
5. G. Liu, Y. Zhang, Z. Ni and R. Huang, *Constr. Build. Mater*., 115(2016)1.
6. Z.Q. Jin, W. Sun, Y.S. Zhang, J.Y. Jiang and J.Z. Lai, *Cem. Concr. Res*., 37(2007)1223.
7. A.K. Tamimi, J.A. Abdalla and Z.I. Sakka, *Constr. Build. Mater*., 22(2008)829.
8. M. El-Hawary, H. Al-Khaiat and S. Fereig, *Cem. Concr. Res*., 30(2000)259.
9. H. Yu, B. Da, H. Ma, H. Zhu, Q. Yu, H. Ye and X. Jing, *Ocean Eng*., 135(2017)1.
10. Y. Yue, J.J. Wang, P.A.M. Basheer and Y. Bai, *Cem. Concr. Compos*., 86(2018)306.
11. Z. Liu, W. Chen, Y. Zhang and H. Lv, *Constr. Build. Mater*., 120 (2016) 494.

12. R. Liu, L. Jiang, G. Huang, Y. Zhu, X. Liu, H. Chu and C. Xiong, *Constr. Build. Mater*., 113 (2016) 90.
13. S. Mundra, M. Criado, S.A. Bernal and J.L. Provis, *Cem. Concr. Res*., 100 (2017) 385.
14. U. M. Angst and B. Elsener, *Sci. Adv*., 3(2017)e1700751
15. J. Zhang, C. Shi, Z. Zhang and Z. Ou, *Constr. Build. Mater*., 152 (2017) 598.
16. H.A.F. Dehwah, S. A. Austin and M. Maslehuddin, Cem. Concr. Res., 54(2002)355.
17. H.A.F. Dehwah, M. Maslehuddin and S.A. Austin, *Cem. Concr. Compos*., 24 (2002) 17.
18. T.P. Cheng, J.T. Lee and W.T. Tsai, *Cem. Concr. Res*., 20 (1990) 243.
19. V. Padilla, P. Ghods and A. Alfantazi, *Constr. Build. Mater*., 40 (2013) 908.
20. N.R. Jarrah, O.S.B. Al-Amoudi, M. Maslehuddin, O.A. Ashiru and A.I. Al-Mana, *Constr. Build. Mater*., 9 (1995) 97.
21. A.J. Al-Teyyib, S.K. Somuah, J.K. Boah, P. Leblanc and A.I. Al-Mana, *Cem. Concr. Res*., 18 (1988) 774.
22. A.J. Al-Tayyib and M. S. Khan, *Cem. Concr. Compos*., 13(1991) 123.
23. F. Shaheen and B. Pradhan, *Cem. Concr. Res*., 91(2017)73.
24. F. Shaheen and B. Pradhan, *Constr. Build. Mater*., 101 (2015) 99.
25. M.A. Espinosa-Medina, G.C.L. Torre, A.S. Castillo, C. Ángeles-Chávez, T. Zeferino-Rodríguez and J.G. González-Rodríguez, Int. J. Electrochem. Sci., 12 (2017) 6952.
26. L.B. Niu and K. Nakada, Corros. Sci., 96 (2015)171.
27. L.B. Niu, K. Okano, S. Izumi, K. Shiokawa, M. Yamashita and Y. Sakai, *Corros. Sci.*, 132 (2018) 284.
28. J. Wu, X. Li, C. Du, S. Wang and Y. Song, *J. Mater. Sci. Technol*., 21(2005)28.
29. J. Williamson and O. B. Isgor, *Corros. Sci*., 106(2016) 82.
30. D. Song, J. Jiang, W. Sun, H. Ma, J. Zhang, Z. Cheng, J. Jiang and Z. Ai, *J. Wuhan Univ. Technol., Mater. Sci. Ed.*, 32(2017)1453.
31. G. Liu, Y. Zhang, M. Wu, R. Huang, *Constr. Build. Mater*., 157 (2017) 357.
32. Z. Jin, X. Zhao, T. Zhao, B. Hou and Y. Liu, *Chin. J. Oceanol. Limnol*., 35(2017)681.
33. M. Stern and A.L. Geary, *J. Electrochem. Soc*., 104(1957)56.
34. C. Andrade and J.A. González, *Mater. Corros.*, 29(1978)515.
35. N. Mursalo, M. Tullmin and F.P.A. Robinson, *J. S. Afr. Inst. Min. Metall*., 88(1988)249.
36. G. Singh, *Int. J. Mine Water*, 5(1986)21.
37. L. Zha, H. Li, N. Wang, S. Lin and L. Xu, *Int. J. Electrochem. Sci*., 12(2017)5704.
38. L. Yang, Y. Xu, Y. Zhu, L. Liu, X. Wang and Y. Huang, *Int. J. Electrochem. Sci.*, 11(2016)6943.
39. J. Wu, K. Pang, D. Peng, J. Wu, Y. Bao and X. Li, *Int. J. Electrochem. Sci.*, 12(2017)1216.
40. S.M. Abd El Haleem, S. Abd El Wanees and A. Bahgat, *Corros. Sci*., 75(2013)1.
41. S.A. El Haleem, S.A. El Wanees, E.A. El Aal and A. Diab, *Corros. Sci*., 52(2010)292.
42. E.E. Abd El Aal, S.A. Abd El Wanees, A. Diab and S.M. Abd El Haleem, *Corros. Sci*., 51(2009)1611
43. D. D. Macdonald, *Electrochim. Acta*, 51(2006)1376.
44. J.B. Jorcin, M.E. Orazem, N. Pébère and B. Tribollet, *Electrochim. Acta*, 51(2006)1473.
45. S. Surviliene, A. Lisowska-Oleksiak and A.Češuniene, *Corros. Sci.*, 50 (2008)338.
46. X. Zhang, S.O. Pehkonen, N. Kocherginsky and G.A. Ellis, *Corros. Sci*., 44 (2002) 2507.
47. M. E. Orazem and B. Tribollet, Electrochemical impedance spectroscopy, John Wiley & Sons, (2008) New York, USA.